Plasma Physics and
Controlled Fusion

Velocity modulations in view of the elliptical approach at Wendelstein 7-X

To cite this article: A Krämer-Flecken *et al* 2025 *Plasma Phys. Control. Fusion* **67** 055024

OPEN ACCESS
IOP Publishing
Plasma Physics and Controlled Fusion
Plasma Phys. Control. Fusion **67** (2025) 055024 (13pp)
https://doi.org/10.1088/1361-6587/adcd2e

Velocity modulations in view of the elliptical approach at Wendelstein 7-X

A Krämer-Flecken[1,*], X Han[2], G Weir[3], T Windisch[3], H M Xiang[1,4], T Andreeva[3], A Dinklage[3], G Fuchert[3], J Geiger[3], J Huang[1,5], S Vaz Mendes[3], K Rahbarnia[3], G Wurden[6] and the W7-X Team[7]

[1] Forschungszentrum Jülich GmbH, IFN-1 - Plasma Physics, D-52425 Jülich, Germany
[2] University of Wisconsin - Madison, Madison, WI 53706, United States of America
[3] Max Planck Institut für Plasmaphysik, D-17491 Greifswald, Germany
[4] Shenzhen Institute of Research and Innovation, University of Hong Kong, Shenzhen 518172, People's Republic of China
[5] Institute of Plasma Physics, Chinese Academy of Sciences, 230031 Hefei, Anhui, People's Republic of China
[6] Los Alamos National Laboratory, Los Alamos, NM 87545, United States of America

E-mail: a.kraemer-flecken@fz-juelich.de.

Received 12 February 2025, revised 8 April 2025
Accepted for publication 15 April 2025
Published 28 April 2025

Abstract

The estimation of the poloidal velocity of the turbulence and the poloidal mean flow velocity are important quantities for the study of sheared flows on turbulence and transport. The estimation depends on the underlying model of the turbulence. Beside the propagation time of the turbulence, its decay with the fading time must be considered. For the description of the propagation, the elliptical approach (EA) is applied, which takes into account the propagation and fading time of the turbulence. The model has been applied successfully in experimental fluid dynamics and is confirmed by direct numerical simulations, also. In this paper, the EA is applied in the analysis of density fluctuations, measured by poloidal correlation reflectometry at two different fusion devices, TEXTOR and W7-X. For the latter, it is demonstrated that the EA is necessary for a correct description of the turbulence propagation. In addition, the velocity modulations are investigated, which in principle can be either generated by an oscillation of the propagation time of density fluctuations and/or an oscillation of the fading of the turbulence. An example for low frequency velocity oscillations in W7-X will be given in the paper, showing a relation between turbulence properties and small oscillations on the measured diamagnetic plasma energy.

Keywords: reflectometry, turbulence propagation, elliptical approach, velocity modulations

---

[7] See Klinger *et al* 2019 (https://doi.org/10.1088/1741-4326/ab03a7) for the W7-X Team.

[*] Author to whom any correspondence should be addressed.

1. Introduction

In a magnetic confined plasma, the radial electric field (E_r) is an important quantity in neoclassical transport analysis [1]. It has a strong impact on radial transport of main ions as well as on impurities [2]. From experimental point of view the measurement of E_r is performed by either heavy ion beam probes [3] in the core of a plasma, where density profiles become flat, reflectometry [4] in the gradient region and probes [5] in the scrape-off-layer (SOL). In case of reflectometry, E_r is obtained from the poloidal propagation of turbulence structures in the plasma, and, with the general assumption that the turbulence phase velocity is negligible compared to the plasma mean flow. This assumption has to be tested carefully before expressing the radial electric field as $E_\mathrm{r} = v_\perp \times B$, where B denotes the local magnetic field. The radial range for applying the different diagnostic is partly overlapping, allowing for a cross validation under special plasma conditions. Of large interest is the transition from the region of closed magnetic field lines, in general the plasma core, to the region of open magnetic field lines, the SOL. At the transition, E_r changes sign and a shear layer is formed in E_r and as well in $v_\perp$. This enhances the suppression of turbulent transport due to shearing apart the eddies in the shear layer, where the radial size of a single eddy is comparable to the radial width of the shear layer.

This region is mainly investigated by reflectometry. Two different flavors of reflectometry exists: (i) Doppler reflectometry [6] and (ii) poloidal correlation reflectometry (PCR) [7–9]. The first one uses the Doppler shift, generated by density fluctuations propagating on a flux surface. The latter one estimates the poloidal turbulence velocity of density fluctuations from a set of poloidally separated receivers using cross correlation techniques. Whereas Doppler reflectometry can resolve different wave numbers, PCR is sensitive to a wave number range $k_\perp \leqslant 3.5\,\mathrm{cm}^{-1}$. In the following, the assumptions and requirements for the velocity estimation of eddies, measured by PCR, are revisited and consequences for the measurement of fluctuations in the plasma flow are discussed. The conditions for application of the Taylor model and its break-down in the vicinity of boundaries are discussed in section 2. In section 3 the elliptical approach (EA) is applied for two different devices, the tokamak TEXTOR [10] and the stellarator W7-X [11], demonstrating a clear need for the EA in W7-X. The implication on velocity oscillations is presented in section 4. In the EA it is shown that oscillations in the velocity can be either due to the oscillation of the propagation time, only, but, also to oscillations in the turbulence properties. For a plasma discharge from W7-X the method is applied and results for the main flow and its oscillations are discussed as well as implications on the diamagnetic energy of the plasma. Section 5 summarizes the findings and gives an outlook for future applications.

2. The EA

Space-time correlations have been used since decades to estimate propagation speeds of turbulent flows. It was demonstrated that the mean velocities are scale independent in a region where no boundaries exist [12]. However, approaching walls will yield a larger mean flow velocity than expected. Especially in this region, the analysis from multiple coherent structures breaks down, as shown in [13]. In fusion plasmas, the role of a wall in a diverted edge plasma is taken by the shear layer, where the mean flow velocity is changing its sign on a short radial range. In Taylor's model, a constant convection velocity of the turbulent eddies is assumed therefore, shearing- and nonlinear terms are ignored. In a space time diagram, contour lines are therefore straight lines. This is also known as frozen turbulence approach. In contrast, the EA is based on two characteristic velocities, which characterize the convection of the flow and its distortion due to the shear effect [14, 15]. In this model the turbulence is non-frozen and in the space time diagram described by elliptical contour lines. In figure 1 the space time diagrams for both models are shown.

In Taylor's model, the convection of the flow is described by:

$$v_\perp = \frac{s}{\Delta t} \tag{1}$$

where s denotes a distance between receivers and Δt the time when the cross correlation function (CCF) has its maximum. In the EA, the two quantities describing the contours are (i) the convective velocity and (ii) the fading velocity [16]. They are given by the following equations:

$$v_\perp = \frac{s\Delta t}{\Delta t^2 + \tau_0^2} \tag{2}$$

$$v_\mathrm{fad} = \frac{s}{\sqrt{\Delta t^2 + \tau_0^2}}. \tag{3}$$

In the above equations τ_0 denotes the time when the mean auto-correlation function (ACF) of the two receivers for a given antenna combination equals the value of the cross-correlation of the two receivers.

To compare the convective velocities in both models, the following calculation is performed, assuming a set of six receivers with increasing distance and equally spaced. With increasing poloidal distance Δt will increase linearly from $1\,\mu$s to (numerical range) $6\,\mu$s. Furthermore, a decay of the turbulence is assumed described by a Gaussian with a $1/e$ width of $5\,\mu$s describing the decay of the turbulence with increasing distance. The half width (σ) of the ACF and CCF in this example is set to $1\,\mu$s. The result is shown in figure 2 left side, where the decrease of the CCF with increasing distance is clearly visible. The colored dots denote the estimated Δt values and the squares the estimated τ_0. The ACF is denoted by a dashed black line. The calculation is repeated, but with a width of the ACF and CCF set to $\sigma = 4\,\mu$s (see right side of figure 2). In this case τ_0 is in the same order as Δt and the ACF is overlapping with the CCF. This will have an effect on the estimated convective velocity. This effect is demonstrated in figure 3. The ×-symbols with the dashed line display the values from the CCF, only. The slope of this curve is the velocity obtained in Taylor's model. Calculating the corrected delay time $\Delta t_\mathrm{c} =$

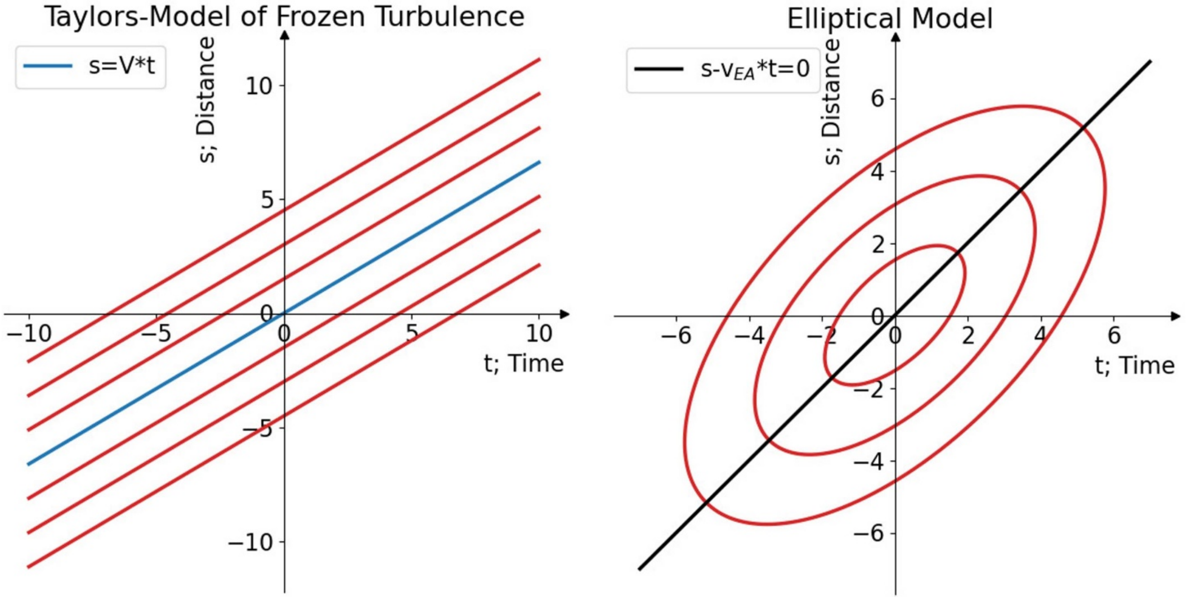

Figure 1. Space time diagram for the Taylor model on the left and the elliptical approach on the right.

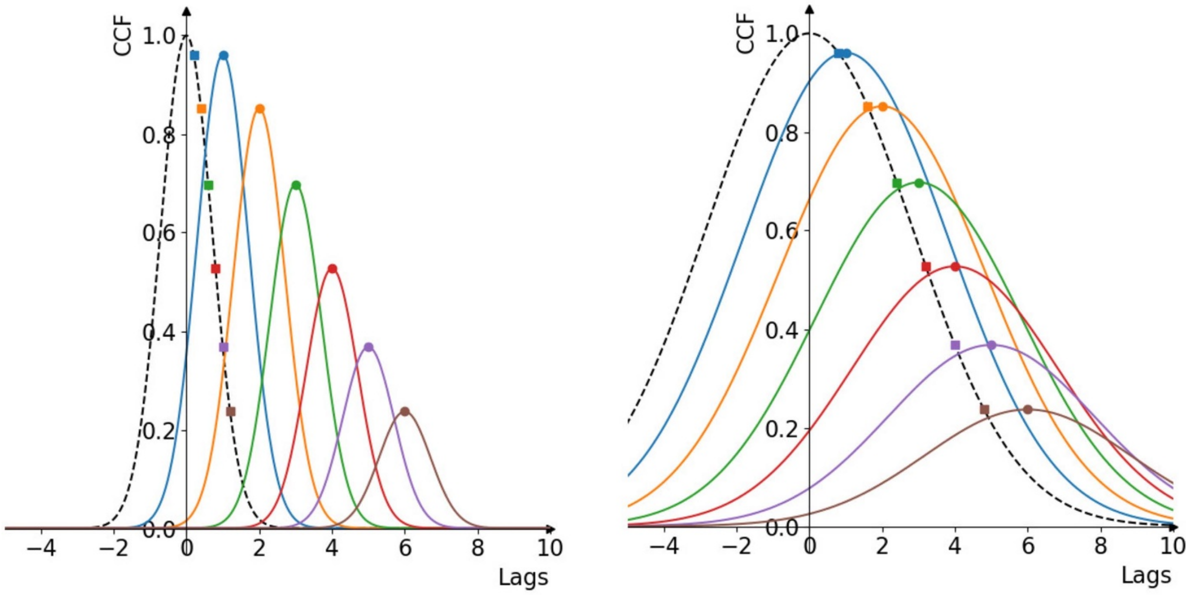

Figure 2. CCF calculation for two cases: (i) $\sigma_{\mathrm{ACF}} = 1\,\mu$s shown on the left and (ii) $\sigma_{\mathrm{ACF}} = 4\,\mu$s shown on the right. Note in both cases the Δt-values are the same. Δt is denoted by circles and τ_0 by squares. The ACF is denoted as black dashed line.

$\Delta t/(\delta t^2 + \tau_0^2)$ yields similar values (orange ■-symbols and solid line). Also, the fading time $\Delta t_{\mathrm{f}} = \sqrt{\Delta t^2 + \tau_o^2}$ (green ■-symbols and dash-dotted line) exhibits a similar increase of the delay with increasing distance between the receivers, concluding that the velocity obtained from the EA is similar to the one from Taylor's model. In case $\sigma = 4.0$, the corrected delays (red ■-symbols and solid line) are larger in the EA and the slope is steeper, yielding a smaller velocity, even if the delays from the CCF-analysis are equal. The reason is the increase in the fading time. Calculating for both cases, $\sigma = 1$ and $\sigma = 4$, $v_\perp$ yields a reduction of $\approx 60\%$ in the case of $\sigma_{\mathrm{ACF}} = 4\,\mu$s. From figure 2 it can be concluded that a ratio $\Delta t/\tau_0 = 5$ for all combinations will change the flow by less than 10%. As long as this condition is fulfilled, the Taylor model is still applicable.

The effect of the EA on the velocity oscillation is according equation (2) twofold; (i) type 1 oscillations are pure oscillations of the delay estimated from the CCF and (ii) type 2 define oscillations of τ_0, indicating oscillation in the turbulence

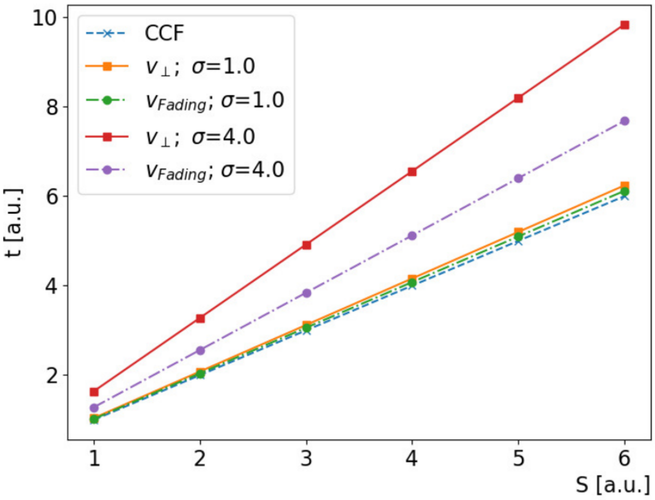

Figure 3. Distance - delay diagram, showing the delays from the CCF-analysis, the corrected delays according to the elliptical approach and the fading time. Clearly seen is the effect of the increased half width of the ACF on the corrected delays and the velocity calculation.

properties. The common understanding of velocity oscillations mean type 1 oscillations with oscillations in Δt, only. In addition to the two extreme cases, a superposition of both types is possible, too. Whereas the oscillations in τ_0 are pointing toward changes in the turbulence properties, as there are the poloidal correlation length $L_\perp \sim | v_\perp | \sigma_{\mathrm{ACF}}$ and the decorrelation time (τ_{dc}). The relation between τ_0 and σ_{ACF} is obvious and can be expressed by:

$$\tau_0 = \sqrt{\frac{\ln\left(\mathrm{CCF}\left(\Delta t\right)\right)}{\ln\left(2\right)}}\,\sigma_{\mathrm{ACF}}. \tag{4}$$

It shows the influence of the poloidal correlation length on the propagation. This will be discussed in section 4 in more detail.

3. Application at TEXTOR and W7-X

Both devices are quite different, TEXTOR was a limiter tokamak with circular poloidal cross-section and W7-X is the largest stellarator in the world and equipped with an island divertor [11]. On both devices, a PCR [8, 9, 17, 18] was/is installed for the measurement of the poloidal turbulence velocity [19]. It has been operated in *Ka*-band with O-mode polarization at TEXTOR and a copy of this system is in operation at W7-X. In O-mode polarization, the probing frequency (22 GHz to (numerical range) 40 GHz) of the PCR is reflected at a radius in the plasma, where the probing frequency equals the plasma frequency. The antenna head of the PCR consists in both devices of five antennae in two adjacent rows. The first one with three vertically arranged antennae has the launcher in the middle, the second row has two further vertically arranged antennae. The antennae in the 2nd row are displaced by half the antenna height in vertical direction. In figure 4 the inlet shows the antennae head as it is installed at W7-X and used in the first three campaigns. The arrangement of the antennae at TEXTOR and W7-X is similar, except a larger antenna mouth in the TEXTOR case, and yields six different antenna combinations. In figure 4 the measurement of Δt and τ_0 for both devices is shown. The plasma parameters for both discharges are different, but for showing the influence of the fading on the propagation, similar plasma parameters are not necessary. The CCFs on the left side are obtained for an ohmic discharge at TEXTOR and those on the right side are obtained for an ECRH heated plasma in W7-X. The obtained delay times from the CCF are in both devices negative, indicating that the measurement is performed in the plasma core. Due to the larger antennae mouth for TEXTOR the poloidal distance is increase by a factor 1.2 for all combinations. The estimated delay from the CCF for the antenna combination **DE** amounts to $-6.1\,\mu$s and in the case of W7-X $\Delta t = -1.7\,\mu$s. The difference is larger than the expected increase due to the larger poloidal distance at TEXTOR, indicating a larger poloidal turbulence propagation in the W7-X case. The poloidal size of the turbulence is proportional to the half width of the ACF. For TEXTOR a half width of $\sigma_{\mathrm{ACF}} = 3\,\mu$s and $\tau_0 \ll \Delta t$. In this case, the Taylor model is still applicable. In case of W7-X a fast propagation is observed together with $\sigma_{\mathrm{ACF}} = 4\,\mu$s, which needs the EA for a correct estimation of the turbulence velocity. The observed accumulation of measurements for the antennae combinations *EC*, *DE*, *BE* and *DC*, *BC* in case of W7-X, comes from the different pitch angle of the magnetic field in both devices. The increased width and faster propagation, for the W7-X case, makes the EA the right tool to estimate the turbulence velocity in W7-X. The two cases show that ACF and CCF have to be checked careful to decide which model is appropriate for the turbulence velocity estimation.

With respect to the velocity estimation, the temporal/radial evolution of the quantities entering equation (2) are shown in figure 5 for W7-X. Here, one full frequency scan of the *Ka*-band is shown. The scan covers the range of 22 GHz to (numerical range) 40 GHz with frequency steps of 0.5 GHz, each step lasting for 20 ms. In this example, the scan covers the radial range of SOL and plasma edge. The CCF is performed every 1 ms yielding Δt, shown in the upper panel, the width of the ACF (σ_{ACF}) is shown in the middle panel and τ_0 in the bottom panel. The calculated Δt is positive and constant in the SOL within the time interval 11.4 s to (numerical range) 11.9 s. After passing the shear layer (abbreviated with S.L. in figure 5(a), the values are negative but constant as well. For σ_{ACF} quite large values are observed in the SOL and the values are decreasing towards the shear layer. In the shear layer, the scatter in σ_{ACF} is largest. In the plasma edge, the values are smaller and constant, showing significant less scatter. A similar development is observed for τ_0. In the SOL, the values are decreasing from $9\,\mu$s to $3\,\mu$s. In the shear layer they are slightly increased and stay around $3\,\mu$s in the plasma edge. The temporal evolution shows that the turbulence properties reflected by the width of the ACF undergo variations, even if Δt shows no variation, as seen in the SOL. As a consequence, the turbulence properties will have an impact on the velocity as calculated by the EA.

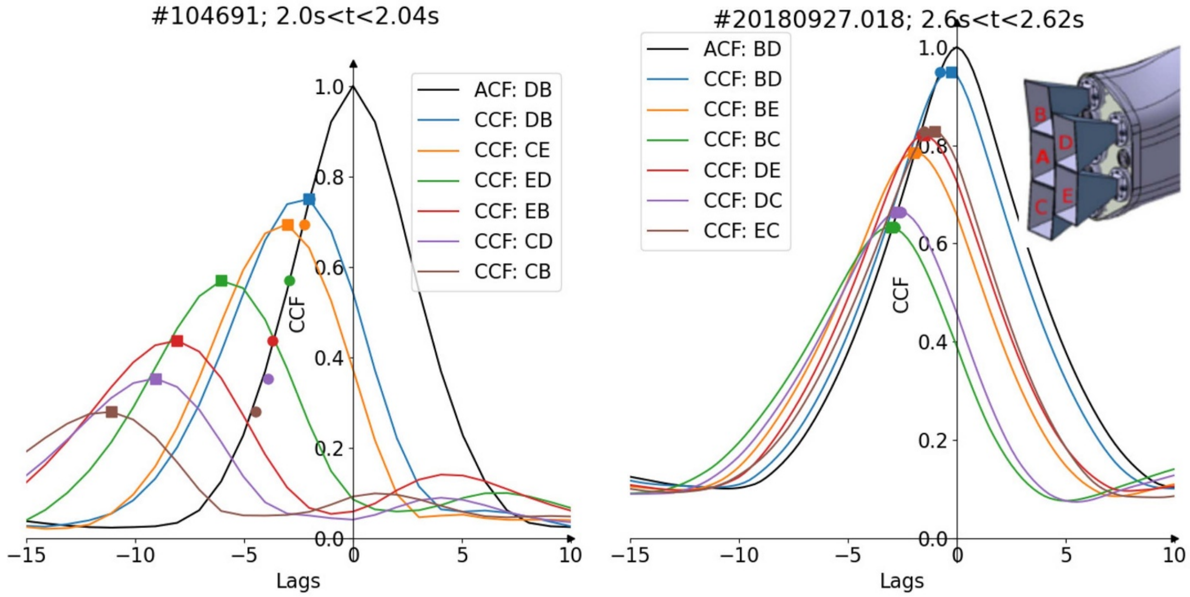

Figure 4. CCF for two examples: (i) left case limiter tokamak TEXTOR and (ii) right case, an example from W7-X. Clearly seen is the difference in σ_{ACF} and the higher rotation in W7-X. At W7-X Δt and τ_0 are comparable, and it is necessary to apply EA for flow estimation.

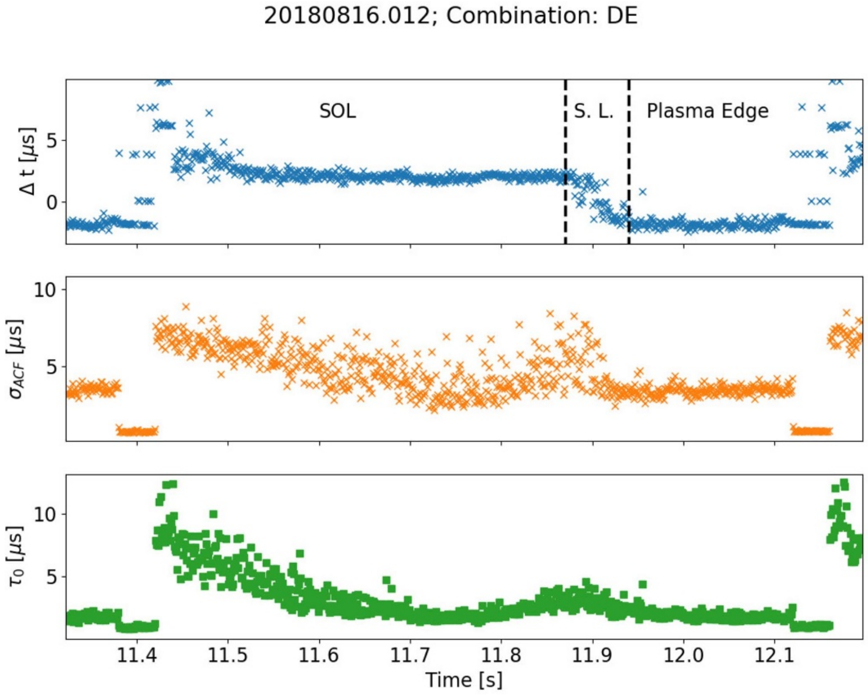

Figure 5. Quantities Δt (upper panel), σ_{ACF} (middle panel), τ_0 (lower panel) for a scan for the PCR in W7-X covering SOL, shear layer and plasma edge. Beside a constant Δt in the SOL and plasma edge, the other quantities show a strong variation and fluctuation in the SOL and shear layer.

4. Velocity oscillations at W7-X - an example

This section discusses the calculation of the turbulence velocity for the W7-X program *20 180 927.018* (see figure 6). For this example the magnetic configuration was not in the standard configuration, with an island chain outside the last closed flux surface (LCFS), but in the so called FNM-configuration, where the 5/5-island chain is located in the plasma edge close to the LCFS. It is characterized further by a constant heating of 2 MW through all the discharge and a line averaged density of $3 \times 10^{19}\,\text{m}^{-2} \leqslant \int n_\text{e}\text{d}l \leqslant 4 \times 10^{19}\,\text{m}^{-2}$ for $t > 1\,\text{s}$. During the discharge, the plasma current (I_p), measured by 8 segmented Rogowski coils, increases from 0 kA to (numerical range) 1 kA and shows fluctuations. A dominant fluctuation frequency of $\approx 250\,\text{Hz}$ is found in the power spectral density (PSD) of I_p [20]. This frequency is also seen in the

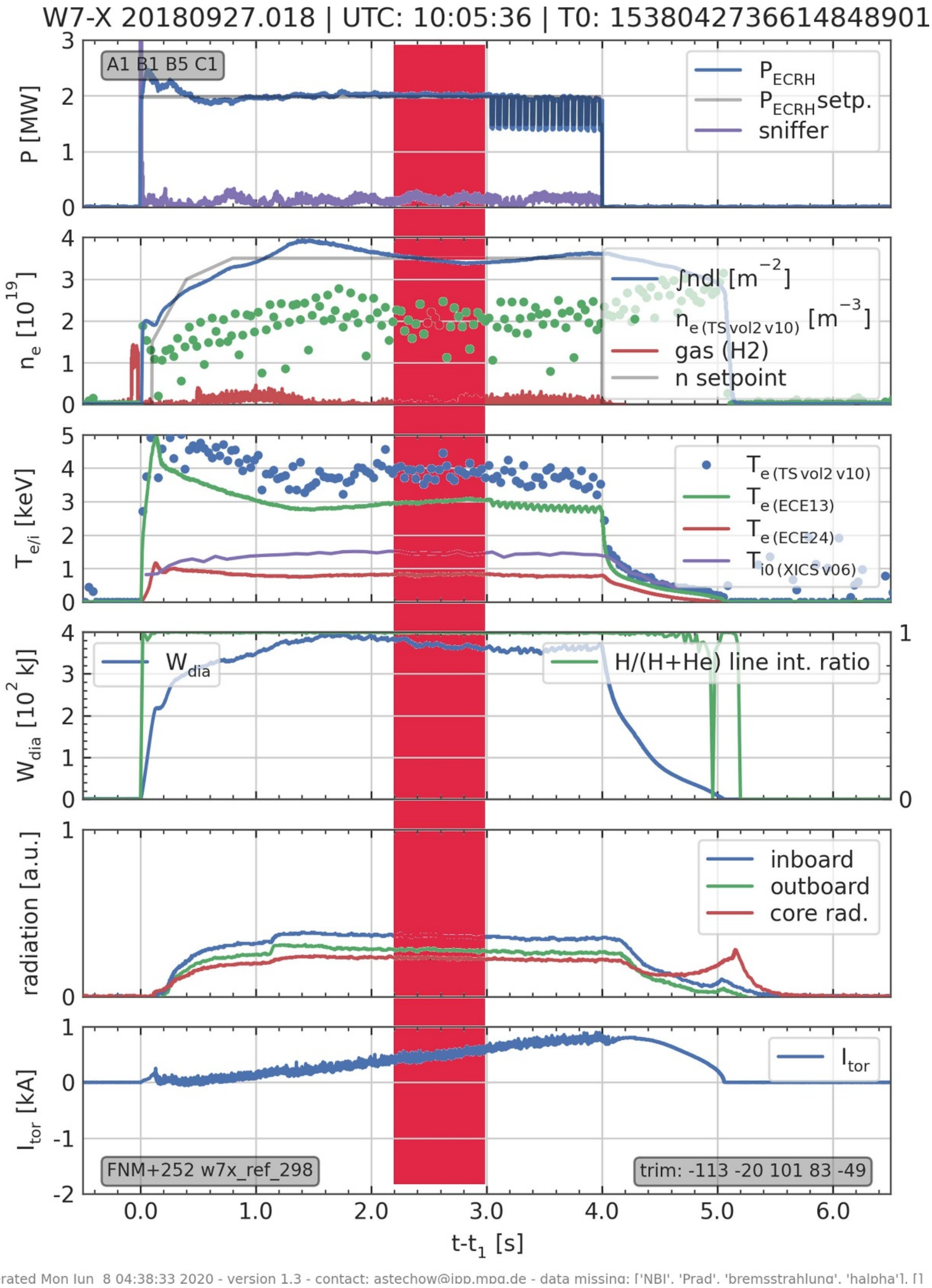

Figure 6. Overview of the temporal evolution of main plasma parameters for program *20 180 927.018*. The red rectangular area marks the time interval for which the analysis of velocity oscillation is performed.

diamagnetic energy (W_{dia}) and has therefore an effect on the confinement. In figure 7, the time trace of the total plasma current and the diamagnetic energy are shown for the time interval 2.7 s to (numerical range) 2.76 s within the flat top phase of the discharge, showing a line averaged density of $n_{\mathrm{e}} \approx 3.5 \times 10^{19}\,\mathrm{m}^{-2}$ as shown in figure 6. In figure 7 the oscillation in both signals is seen clearly. The red dashed lines indicate that the oscillations are in phase during the full-time interval, except for a smoother modulation in W_{dia}, than in I_{p}. From the time trace of W_{dia}, it can be seen that the fluctuation contribute with $\leqslant 1\%$ to the signal amplitude for the investigated time interval.

The analysis of the data from PCR is restricted to a quite flat top phase of the program, as indicated by the red rectangular area in figure 6. Within the flat top, one full frequency scan of the diagnostic is analyzed. In the sequence of repetitive

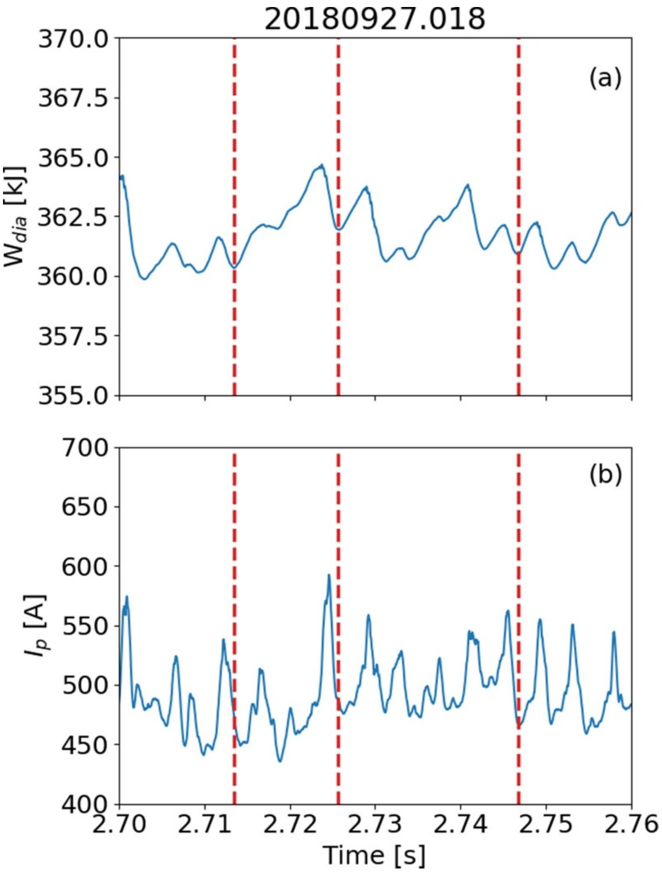

Figure 7. Time trace of total plasma current (a) and diamagnetic energy (b) for a small time window during the scan of the PCR. It shows an oscillation with a period of 4 ms. The dashed vertical lines indicate that the minima in the oscillations of W_{dia} are related to the minima in the plasma current signal.

scan, it has the number 3 and corresponds to the time interval $2.22\,\mathrm{s} \leqslant t \leqslant 2.96\,\mathrm{s}$. The analysis of the PSD from PCR yields of σ_{ACF} and Δt for all antenna combinations is shown in figure 8. A clear 250 Hz peak in σ_{ACF} is observed in all combinations. The same peak is observed in Δt, however, at a smaller amplitude and not as pronounced as in σ_{ACF} and with a reduced spectral width. It indicates that the poloidal size of the turbulence is mainly affected. From the calculation of the turbulence velocity (see figure 9) applying the EA for time steps of 1 ms, the shear layer and the plasma edge are well recognized. In the shear layer $v_\perp$ decreases and in the plasma edge for, $t > 2.48\,\mathrm{s}$ corresponding to a cut-off density of $n_\mathrm{e} \geqslant 1.2 \times 10^{19}\,\mathrm{m}^{-3}$, the turbulence velocity exhibits a large fluctuation amplitude, which is in the order of $\tilde{v}_\perp \approx 3\,\mathrm{km\,s}^{-1}$ to (numerical range) $4\,\mathrm{km\,s}^{-1}$. The error bar of each single measurement is much smaller than the fluctuation amplitude. This observation is caused by the 250 Hz oscillation observed in Δt and σ_{ACF}.

In the next step, the radial localization of the flow oscillations is analyzed. Therefore, a mean density profile, measured by the Thomson scattering diagnostic [21], in the time range of interest is calculated (see figure 10). It is used to map the cut-off density to a reflection radius. It is seen that the fluctuation covers a range of at least 4 cm in the gradient region of the profile, as indicated by the red rectangular area in the figure. The upper boundary of the fluctuation cannot be determined, because it is outside the probing frequency range of the PCR. As mentioned above, the magnetic configuration of this program exhibits an 5/5-island chain inside the LCFS. To relate the measured flow profiles to the magnetic flux surfaces, the field line tracer [22] is used. The Poincaré-map is a representation of the magnetic structure in a poloidal cross-section and for the toroidal position where the PCR is installed. The generation of the Poincaré-map is based on the iota-corrected coil currents database [23] for this configuration in the vacuum case and calculated for the position of the PCR. In figure 11 the Poincaré-map in the radial range of interest is shown. The 5/5-island is centered below the mid-plane. Beside this island, two additional islands belonging to the (10/9)-island chain are observed at the far plasma edge inside the SOL. In between both island chains, the LCFS is located, represented by the dashed orange line. Nearly horizontal dashed lines indicate the line of sight (LoS) of the PCR antennae intersecting the 5/5-island. The intersection of the LoS with the island separatrix is shown in light cyan color. Poloidal velocity profiles are calculated from the data shown in figure 9 by averaging over each frequency step separately. To calculate the profiles for the extreme cases, the colored boxes from figure 9 are used, which fulfill the following conditions: (i) velocity measurements are within the range $-10.5\,\mathrm{km\,s}^{-1}$ to (numerical range) $-6.5\,\mathrm{km\,s}^{-1}$ (red box) and (ii) values in the range $-4.5\,\mathrm{km\,s}^{-1}$ to (numerical range) $-0.5\,\mathrm{km\,s}^{-1}$ (green box). In addition, a mean profile taking into account all measurements is calculated. Within the shear layer the profiles for all three cases look similar, as already seen from figure 9, the fluctuation starts behind the shear layer and before the island structure has been reached, as it is indicated by the Poincaré-map. The profiles cover to some extent the 5/5-island, as can be seen from the LoS of the antennae. However, without a full $v_\perp$-profile, it cannot be decided if the whole plasma column shows this fluctuation or only the edge. An increase of the $v_\perp$-profile in the island region at W7-X is reported by [24] in another limiter configuration with the 5/5-island inside the LCFS. However, the observation described here, shows a dynamic nature of the island structure in the investigated discharge.

The 6 combinations probe different poloidal distances of the receiver antennae. These can be used to get information on the decay of the CCF in terms of decorrelation time and correlation length. In figure 12(a), the maximum of the CCF is shown as a function of the corrected delay time, given by: $\Delta t_{\mathrm{cor}} = (\Delta t^2 + \tau_0^2)/\Delta t$ for the two different velocity intervals, as indicated in figure 9. For this purpose, the measurements are averaged across the radial range where the velocity oscillation is observed. Clearly seen is the scatter in Δt_{cor} for the interval

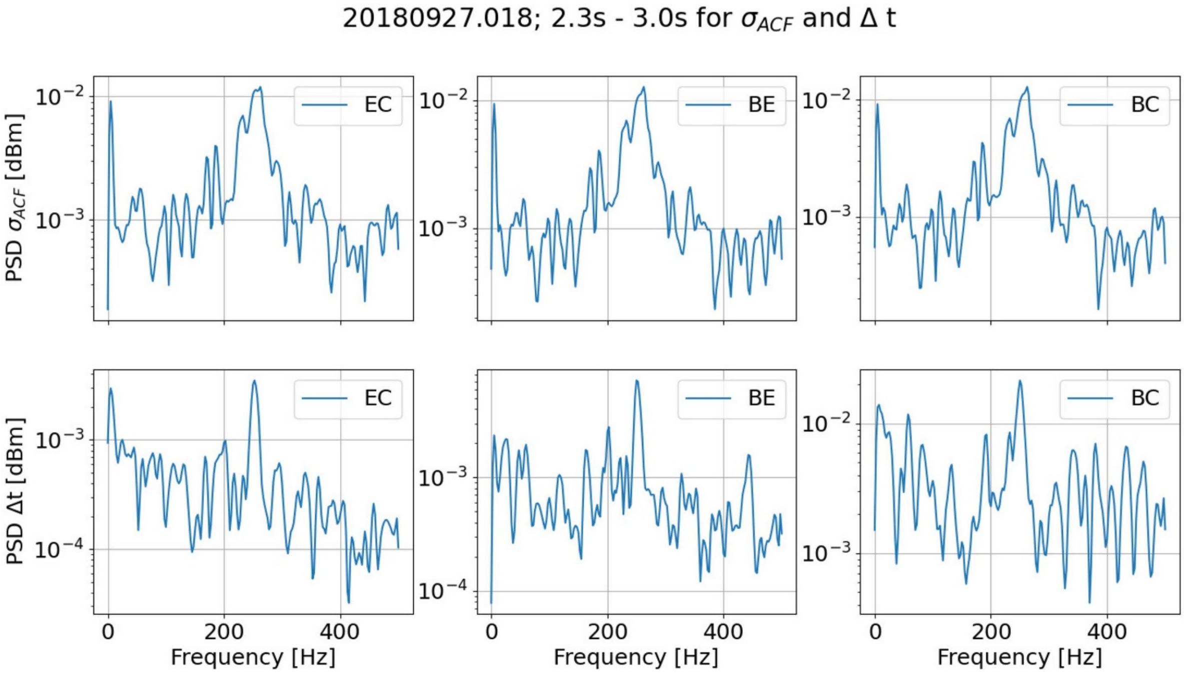

Figure 8. PSD of σ_{ACF} and Δt for three different antenna combinations. For both quantities, all combinations show a fluctuation at 250 Hz. It is weaker in Δt than in σ_{ACF}.

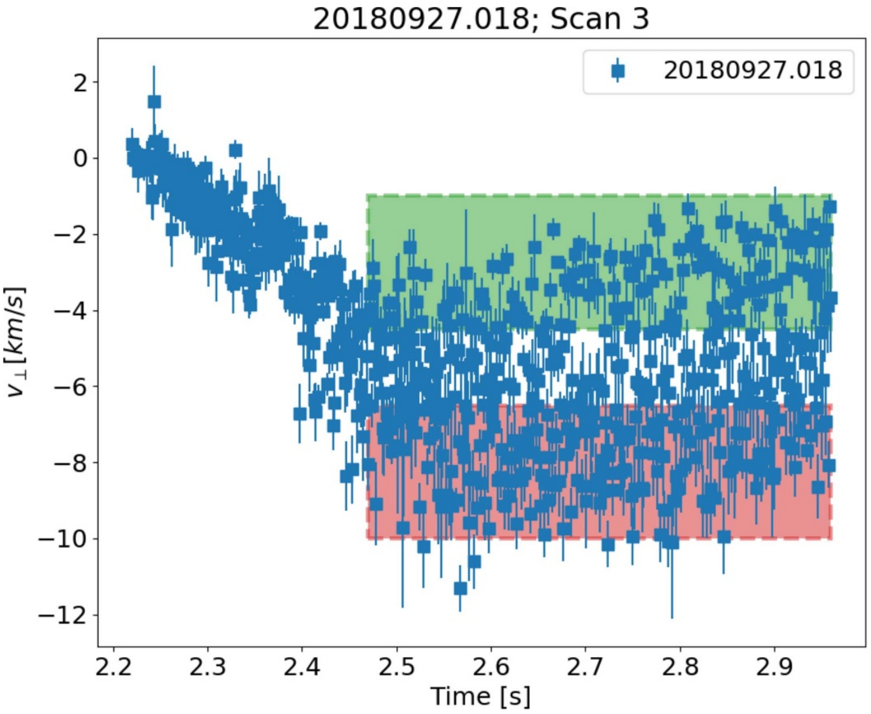

Figure 9. The temporal evolution of the turbulence velocity for a scan of the PCR. Clearly seen is the shear region and in the plasma edge the flow is fluctuating. Two regions are marked: (i) one in red, where the velocity is smallest, and (ii) a green one, where the flow is largest.

$-4.5\,\mathrm{km\,s^{-1}}$ to (numerical range) $-0.5\ \mathrm{km\,s^{-1}}$. For each of both velocity intervals, the data are approached by a Gaussian. The half width at half maximum (HWHM) for the interval $-10.5\,\mathrm{km\,s^{-1}}$ to (numerical range) $-6.5\,\mathrm{km\,s^{-1}}$ is with 5.7 μs a factor of ≈ 2 smaller than the one for -4.5 to (numerical range) $-0.5\,\mathrm{km\,s^{-1}}$ which yields 11.5 μs. Smaller HWHM indicate a faster decay of the turbulence. The time needed to reach the $1/e$-level is defined as the decorrelation time and amounts to 6.8 μs and 13.8 μs, respectively. In figure 12(b) the maximum in the CCF is shown as a function of the poloidal distance. Here, the HWHM for the interval $-10.5\,\mathrm{km\,s^{-1}}$ to (numerical range) $-6.5\ \mathrm{km\,s^{-1}}$ with $\sigma_{ACF} = 0.055\,\mathrm{m}$ is larger compared to the interval $-4.5\,\mathrm{km\,s^{-1}}$ to (numerical range) $-0.5\,\mathrm{km\,s^{-1}}$ yielding a HWHM of 0.045 m, indicating that

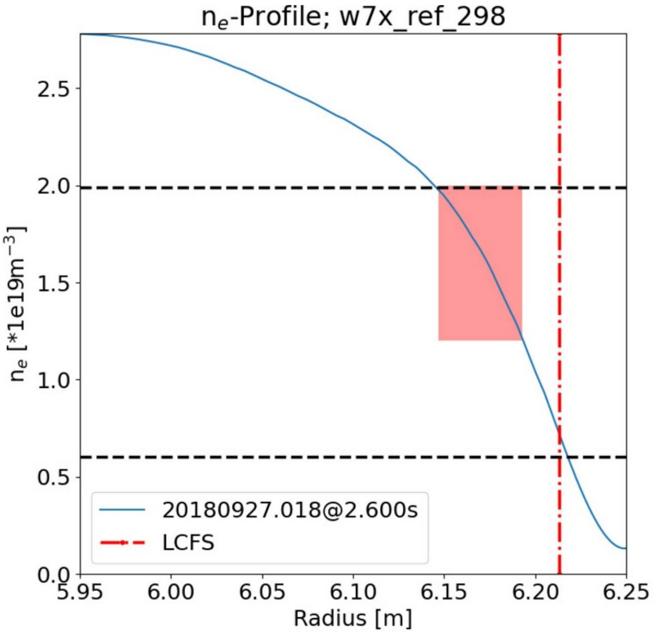

Figure 10. Averaged density profile for scan 3. The range where the fluctuations are visible is denoted by a red rectangular. The LCFS is indicated by a red line and the probed density range is given by dashed horizontal lines.

in the first case the poloidal correlation length is larger. This observation shows that the turbulence undergoes a change, which is unexpected for a pure velocity oscillation, based on changes in the propagation time, only. It is more a signature that the turbulence structure changes, and the observed oscillation could be evidence for the existence of a rotating mode structure with different turbulence properties. this is also evident from the large error bars in Δt_{cor} for the case with reduced $v_\perp$. However, to get more evidence for this hypothesis, additional experiments are necessary.

Beside the estimation of the velocity and its oscillations, the PCR can be used to determine the turbulence spectra. For this purpose, a conditional averaging method is used. In a first step, all time stamps where the measurement is either in the red or green rectangular area are identified (see figure 9). For the PSD a time interval of ±0.5 ms around the time stamp is estimated. On these intervals, also the cross PSD (CPSD) and the coherence are calculated. All spectra are summed up and normalized with respect to the number of measurements in each of the rectangular boxes. The spectra for the antennae combination **DE** probing a poloidal distance of 17 mm are shown in figure 13. A big difference between the spectra for the two velocity intervals is observed for $f \geqslant 16\,\mathrm{kHz}$. In the case of the higher absolute velocity profile (red curves in figure 13 and red box in figure 9), the spectra show a higher power for $f > 16\,\mathrm{kHz}$ and the decay of the spectra is described by more than one slope, compared to the case with lower absolute turbulence velocity (green curves in figure 13 and green box in figure 9), where the decay can be described by one single slope above $f = 16\,\mathrm{kHz}$ (see figures 13 (a)–(c)). The existence of more than one slope indicates an additional energy input into the turbulence spectrum for $16\,\mathrm{kHz} \leqslant f \leqslant 100\,\mathrm{kHz}$. It indicates that turbulence in this frequency range has a strong contribution, which is a commonly accepted fact for increased transport [25]. A quantification of this effect however is difficult and not discussed in this paper. From the coherence spectrum (figure 13 (d)), it can be seen that for the case with higher absolute velocity, the coherence is larger in the range 2 kHz to (numerical range) 400 kHz. Above, $f \approx 140\,\mathrm{kHz}$ both spectra exhibit a similar slope in the decay of the coherence. For the frequency range, $f > 300\,\mathrm{kHz}$ the coherence is small, and the observed PSD in figures 13 (a)–(c) indicates that uncorrelated broad band turbulence with short decay times contribute, mostly.

W7-X is optimized with respect to neoclassical transport. This means that turbulent transport is expected to be dominant. The observation of a reduction in the turbulence spectra, as shown in figure 13, suggest that the observed fluctuations could have an effect on the confinement and diamagnetic energy (W_{dia}). To check this assumption, the CPSD, coherence and cross phase of the oscillation between the flow and W_{dia} is calculated and shown in figure 14. The CPSD as well as the coherence show a clear indication of the 250 Hz fluctuation. Furthermore, the cross phase suggests a phase difference of $176 \pm 9^\circ$. This can be taken as an evidence that the fluctuations in the turbulence velocity have an impact on the diamagnetic energy and confinement, or vice versa. The maximum in W_{dia} is achieved for the higher absolute velocity profile. This observation goes along with an increased shear layer depth, as shown in figure 11. Also, the phase between the turbulence velocity and the plasma current is estimated. It yields a phase difference of $121 \pm 10^\circ$. To identify a possible relation with the $5/5$-island chain, the phase between each single segmented Rogowski coil and $v_\perp$ is calculated. The phase varies between 105° to (numerical range) 160° or -75° to -20°, respectively, when taking into account the negative velocities. The PCR and the segmented Rogowski coils are located at a toroidal angle of 72° and 104°. The phase difference of -35° agrees well with the toroidal separation between both diagnostics, which amounts to 32°. This may be an indication for a modulation of the $5/5$-island size by the plasma current. Since the PCR diagnostic is located poloidally below the equatorial plane, a change in the poloidal size of the island can be observed. The observed modulation in $v_\perp$ could be due to a measurement outside the $5/5$-island, yielding a minimum in the velocity and a slightly increased diamagnetic energy, as well as a decrease in the plasma current. The other extreme, where the poloidal size of the $5/5$-island is increased, goes along with an increased $v_\perp$ and plasma current, while the diamagnetic energy is decreased. These observations suggest that the poloidal size of the $5/5$-island is modulated with a period of 4 ms. Usually such behavior is not a velocity oscillation in a classical understanding, where the background plasma undergoes no or only small changes. In the presented case, the plasma properties change and therefore the measured turbulence velocity. This is also displayed in variation of the turbulence properties.

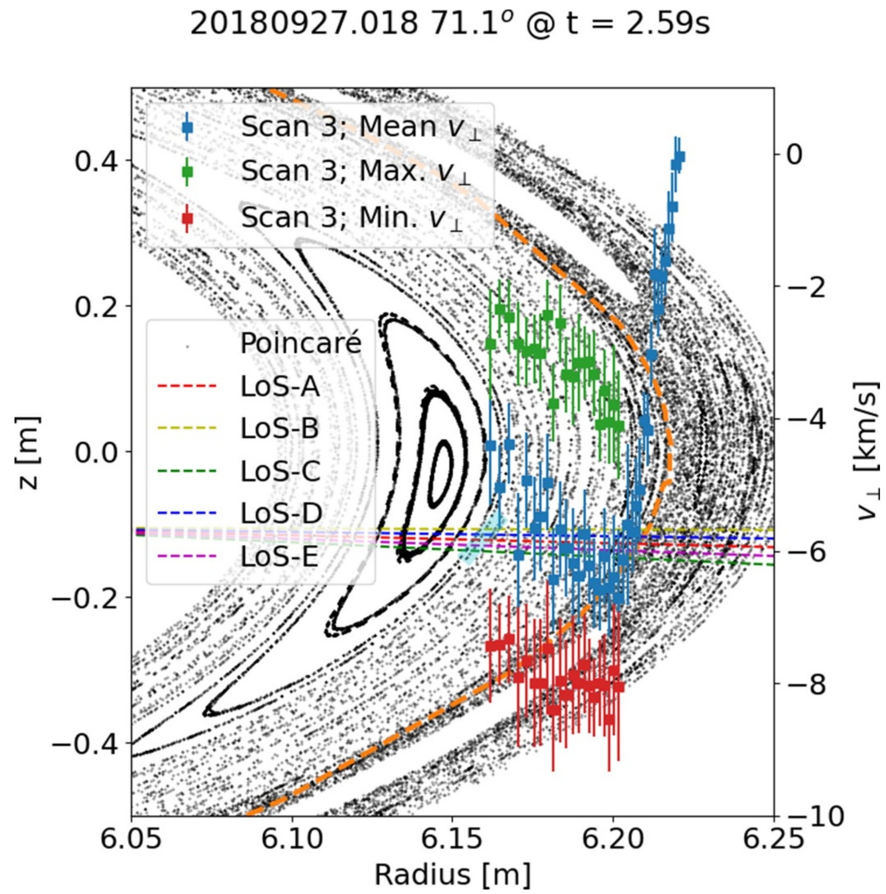

Figure 11. Profiles of the turbulence velocity for the two cases from figure 9 and an averaged profile. The Poincaré map is shown, indicating that the measurement is covering the region of the island, partly. The dashed nearly horizontal lines indicate the LoS of the antenna. The dashed orange line indicates the last close flux surface and the light cyan region indicates the separatrix of the 5/5-island.

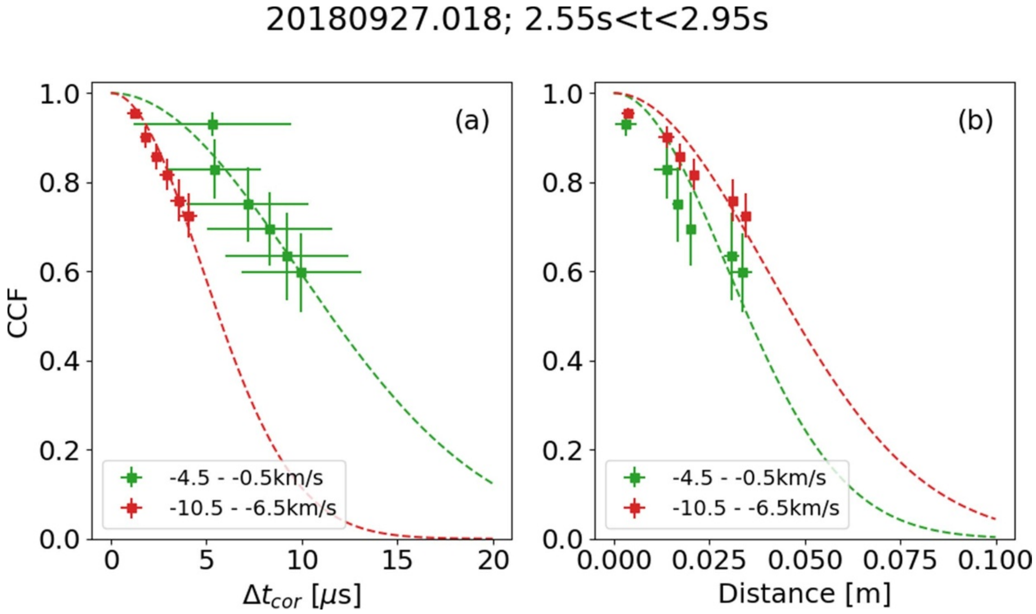

Figure 12. Decay of the maximum in the CCF as (a) a function of the corrected delay time Δt_{corr} and (b) the poloidal distance.

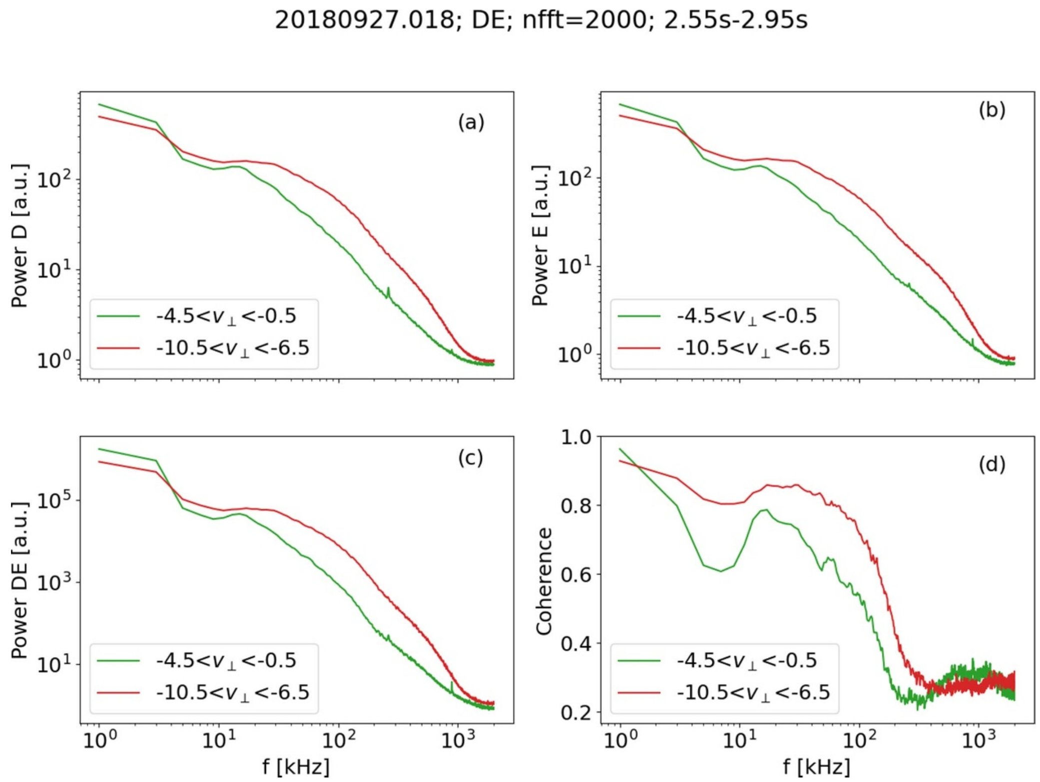

Figure 13. PSD, CPSD and coherence for the antennae combination **DE**. The spectra show a clear difference for time stamps lying within the red rectangular area compared to those lying in the green rectangular area of figure 9.

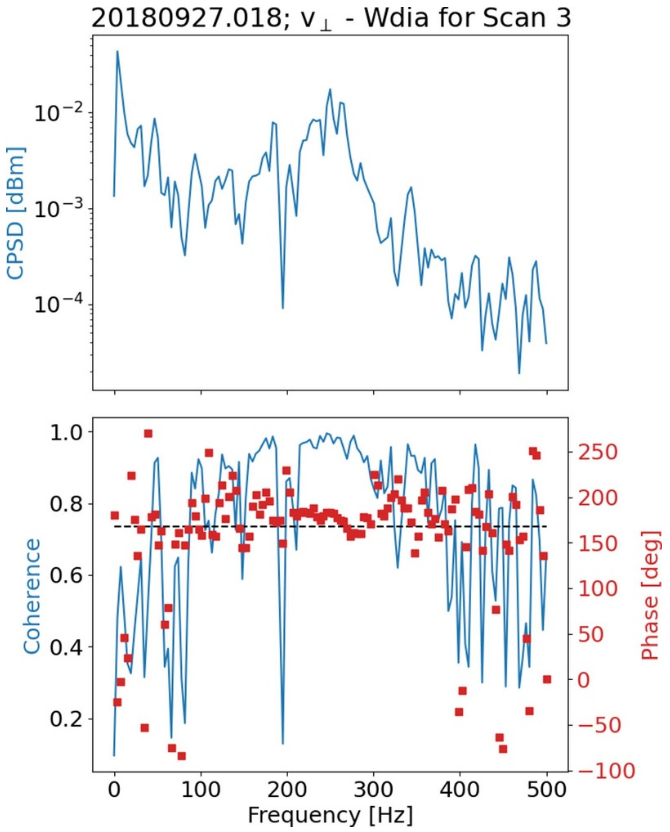

Figure 14. Upper panel show the CPSD of $v_\perp$ versus W_{dia} which shows a peak at $f = 250\,\mathrm{Hz}$. The lower panel shows the coherence and cross phase. A phase of -180° is calculated.

5. Conclusions and outlook

The paper discusses measurements of the turbulence velocity in fusion devices in general. It has been demonstrated that the EA is necessary to describe the turbulence velocity in the plasma edge and especially in the vicinity of a shear layer. In the plasma core and gradient region without the vicinity of a shear layer, the EA will yield a similar estimation of the flow velocity as the Taylor model, as long as the condition $\Delta t \geqslant 5\,\tau_0$ is fulfilled. However, regarding the turbulence velocity oscillations, EA takes into account the turbulence properties which contribute to the velocity with oscillations of τ_0, depending on the half width of the CCF and which is a measure for the poloidal correlation length. The application of the EA will improve the analysis of turbulence propagation in general. It can be applied not only for poloidal correlation reflectometer, as discussed in this publication, but, also for other diagnostics e.g. arrays of probe measurements in the plasma scrape off layer. Furthermore, the improved experimental data analysis using the EA will allow for a better estimation of the flow profiles and the comparison with profiles based on neoclassical theory will become more conclusive.

The EA is applied for a plasma discharge in W7-X, where a low frequency oscillation ($f \approx 250\,\mathrm{Hz}$) in the plasma current is observed. It is shown that these oscillations modulate the poloidal turbulence velocity inside the last closed flux surface. The amplitude of this modulation amounts to $\tilde{v}_\perp \approx 4\,\mathrm{km\,s^{-1}}$. This modulation could be traced back, beside the oscillation of the delay time from the cross correlation, to an oscillation of the decorrelation time and poloidal correlation length of the turbulence. The results indicate that the observed velocity oscillations come from a change of the background plasma, which are different from classical velocity oscillations where the background plasma is not varying. Furthermore, for the investigated discharge, the diamagnetic energy is modulated by $\approx 1\%$ which has an effect on the confinement time. It demonstrates, even if small, that local and radial changes in the turbulence properties are visible in the overall measured diamagnetic energy. Along with this oscillation, a change in the turbulence spectra is observed. It opens a space for further investigations on the origin, causing the oscillation of the plasma current in the edge and the relation to the $5/5$-island chain inside plasma edge and close to the last closed flux surface.

Data availability statement

Data are shared only within the W7-X team and TEXTOR data are stored behind a fire wall and not public accessible The data that support the findings of this study are available upon reasonable request from the authors.

Acknowledgment

This work has been carried out within the framework of the EUROfusion Consortium, funded by the European Union via the Euratom Research and Training Programme (Grant Agreement No 101052200 -EUROfusion). Views and opinions expressed are however those of the author(s) only and do not necessarily reflect those of the European Union or the European Commission. Neither the European Union nor the European Commission can be held responsible for them.

ORCID iDs

A Krämer-Flecken https://orcid.org/0000-0003-4146-5085
X Han https://orcid.org/0000-0001-8498-6433
G Weir https://orcid.org/0000-0002-2370-409X
H M Xiang https://orcid.org/0000-0001-7799-6190
T Andreeva https://orcid.org/0000-0003-2390-4240
A Dinklage https://orcid.org/0000-0002-5815-8463
J Geiger https://orcid.org/0000-0003-4268-7480
J Huang https://orcid.org/0000-0001-6289-1812
S Vaz Mendes https://orcid.org/0009-0004-8162-6626
K Rahbarnia https://orcid.org/0000-0002-5550-1801
G Wurden https://orcid.org/0000-0003-2991-1484

References

[1] Helander P and Sigmar D J 2001 *Collisional Transport in Magnetized Plasmas* (Cambridge University Press)

[2] García-Regaña J M, Kleiber R, Beidler C D, Turkin Y, Maaßberg H and Helander P 2013 On neoclassical impurity transport in stellarator geometry *Plasma Phys. Control. Fusion* **55** 074008

[3] Bondarenko I S *et al* 2001 Installation of an advanced heavy ion beam diagnostic on the TJ-II stellarator *Rev. Sci. Instrum.* **72** 583–5

[4] Schirmer J, Conway G D, Holzhauer E, Suttrop W and Zohm H 2007 Radial correlation length measurements on asdex upgrade using correlation doppler reflectometry *Plasma Phys. Control. Fusion* **49** 1020–41

[5] Andreason S P and Slough J T 2004 Internal probe array for the measurement of radial electric field *Rev. Sci. Instrum.* **75** 4302–4

[6] Conway G D, Schirmer J, Klenge S, Suttrop W and Holzhauer E (The ASDEX Upgrade Team) 2004 Plasma rotation profile measurements using doppler reflectometry *Plasma Phys. Control. Fusion* **46** 951

[7] Vershkov V A, Tuccillo A, Tudisco O M, De Benedetti P, Buratti P, Smeulders D, Shelukhin A and Zonca F (FTU Team) 2001 First results of turbulence measurements in ftu tokamak with heterodyne correlation reflectometer *28th EPS Conf. on Controlled Fusion and Plasma Phys.* vol 25A pp 65–68

[8] Krämer-Flecken A, Soldatov S, Vowinkel B and Müller P 2010 Correlation reflectometry at textor *Rev. Sci. Instrum.* **81** 113502

[9] Krämer-Flecken A, Windisch T, Behr W, Czymek G and Drews P 2017 Investigation of turbulence rotation in limiter plasmas at w7-x with newly installed poloidal correlation reflectometer *Nucl. Fusion* **57** 066023

[10] Neubauer O, Czymek G, Giesen B, Hüttemann P W, Sauer M, Schalt W and Schruff J 2005 Design features of the tokamak textor *Fusion Sci. Technol.* **47** 76–86

[11] Bosch H-S, Wolf R C, Andreeva T, Baldzuhn J and Birus D *et al* 2013 Technical challenges in the construction of the steady-state stellarator wendelstein 7-x *Nucl. Fusion* **53** 126001

[12] Kim J and Hussain F 1993 Propagation velocity of perturbations in turbulent channel flow *Phys. Fluids A* **5** 695–706

[13] Zaman K B M Q and Hussain A K M F 1981 Taylor hypothesis and large-scale coherent structures *J. Fluid Mech.* **112** 379–96

[14] Guo-Wei H and Zhang J-B 2006 Elliptic model for space-time correlations in turbulent shear flows *Phys. Rev. E* **73** 055303

[15] Guo-Wei H, Jin G and Zhao X 2009 Scale-similarity model for lagrangian velocity correlations in isotropic and stationary turbulence *Phys. Rev. E* **80** 066313

[16] Briggs B H, Phillips G J and Shinn D H 1950 The analysis of observations on spaced receivers of the fading of radio signals *Proc. Phys. Soc. B* **63** 106

[17] Krämer-Flecken A, Dreval V, Soldatov S, Rogister A and Vershkov V (The TEXTOR-Team) 2004 Turbulence studies with means of reflectometry at textor *Nucl. Fusion* **44** 1143–57

[18] Windisch T, Krämer-Flecken A, Velasco J L, Könies A and Nührenberg C 2017 Poloidal correlation reflectometry at w7-x: radial electric field and coherent fluctuations *Plasma Phys. Control. Fusion* **59** 105002

[19] Han X *et al* (The W7-X Team) 2021 Application of the elliptic approximation model for the edge turbulence rotation measurement via the poloidal correlation reflectometer in wendelstein 7-x *Nucl. Fusion* **61** 066029

[20] Wurden G A, Bozhenkov S, Fuchert G and Zhang D 2019 A special case of long-pulse high performance operation in w7-x *46th EPS. Conf. on Plasma Physics (Milan, Italy)* (EPS) p 1.118

[21] Pasch E, Beurskens M N A, Bozhenkov S A, Fuchert G, Knauer J and Wolf R C (W7-X Team) 2016 The Thomson scattering system at wendelstein 7-x *Rev. Sci. Instrum.* 87 11E729

[22] Bozhenkov S A, Geiger J, Grahl M, Kißlinger J, Werner A and Wolf R C 2013 Service oriented architecture for scientific analysis at w7-x. an example of a field line tracer *Fusion Eng. Des.* **88** 2997–3006

[23] Andreeva T *et al* (The W7-X Team) 2022 Magnetic configuration scans during divertor operation of wendelstein 7-x *Nucl. Fusion* **62** 026032

[24] Estrada T *et al* (The W7-X Team) 2021 Impact of magnetic islands on plasma flow and turbulence in w7-x *Nucl. Fusion* **61** 096011

[25] FUJISAWA A 2021 Review of plasma turbulence experiments *Proc. Japan Acad. B* **97** 103–19